ADVANCED ENERGY MATERIALS
www.advenergymat.de

Why Half-Cell Samples Provide Limited Insight Into the Aging Mechanisms of Potassium Batteries

Fabian Jeschull, Elmar Kataev, Iurii Panasenko, Christian Njel, Roberto Félix, and Julia Maibach*

Photoelectron spectroscopy (PES) studies of solid electrolyte interphases (SEI) of cycled battery electrodes are mostly performed in half cell configurations (i.e., against metallic counter electrodes). In contrast to less reactive Li metal, problems arise in post-Li systems, like K-ion cells, where crosstalk phenomena strongly interfere with the surface layer formation process. This raises the question of whether surface analysis data from half cell experiments are still representative and transferable to corresponding full cells in post-Li systems. Here the major differences between SEI layers formed on graphite electrodes are outlined in K-ion half and full cells derived from an in-depth surface analysis approach combining in-house and (synchrotron-based) hard X-ray PES. This results highlight significant changes in SEI characteristics, both in terms of SEI layer thickness and gradual compositional changes across the interphase, when K-metal (half cell) is replaced by a Prussian white positive electrode (full cell). Furthermore, the initial SEI layers formed on the first cycle are found to evolve and age differently upon further cycling, depending on the two cell configurations. This study stresses the additional complexity of studying post-Li cells and the need to carefully design surface analysis experiments for meaningful material and electrode interphase characterization.

1. Introduction

Amongst the Group 1 elements, K-ion batteries (KIBs) are the latest addition to the portfolio of energy storage devices. Similar to Na-ion batteries (NIBs), they are potentially cheaper and more sustainable than Li-ion batteries (LIBs) owing to a more abundant raw material basis, provided critical elements such as Ni and Co are avoided. Development of KIBs benefits greatly from accomplishments in material chemistry of Li- and Na-ion technologies. A common cell configuration is graphite[1,2] as negative and Prussian white, $K_2M_{TM}[Fe(CN)_6]$ (M_{TM} = Mn, Fe)[3,4] as positive electrode in combination with carbonate-based electrolytes, which are both prominent electrode materials in LIBs[5] and NIBs.[6] Although K-ions reduce the electrode gravimetric capacity due to their higher atomic mass, this penalty can be offset through higher cell voltages resulting in projected specific energies and energy densities in the range of corresponding Prussian white/hard carbon NIB and $LiFePO_4$/graphite LIB cell configurations.[7]

However, in terms of cycle life KIBs still face major challenges related to the reactivity of potassium and the formation of less protective passivation layers. For the analysis of the solid electrolyte interphase (SEI) ex situ photoelectron spectroscopy (PES) is commonly used for its high surface-sensitivity. Because of the complexity and the thickness of the SEI formed on graphite electrodes in KIB half cells, in-house spectrometers using standard Mg or Al Ka soft X-ray sources reach their limits in probing the entire surface layer. Hence, an in-depth analysis of the complex SEI layer at higher probing depths would be very beneficial and can be realized using hard X-ray photoelectron spectroscopy (HAXPES).

So far there are but a few HAXPES studies on graphite electrodes for KIBs in literature. Naylor et al.[8] reported on the evolution of the SEI layer at different states of charge (SOC) during the first intercalation-deintercalation cycle of K-ions in graphite electrode in half cells. In a HAXPES study by Hosaka et al.[9] the SEI layers formed on cycled graphite electrodes were compared after 10 cycles in both half and full cell setups with carbonate-based electrolyte containing either KPF_6 or potassium bis(fluorosulfonyl)imide (KFSI) as electrolyte salts (the most commonly used electrolyte formulations[10]). Based on previous (in-house) PES[11–13] and correlated gas chromatography-mass spectrometry (GC-MS)[12,14–16] results, half cell results are biased by severe crosstalk events in presence of a potassium metal electrode in the cell. For example, the reaction of

F. Jeschull, I. Panasenko, C. Njel[++], J. Maibach[+]
Institute for Applied Materials – Energy Storage Systems (IAM-ESS)
Karlsruhe Institute of Technology (KIT)
76344 Eggenstein-Leopoldshafen, Germany
E-mail: fabian.jeschull@kit.edu

E. Kataev, R. Félix
Helmholtz-Zentrum Berlin für Materialien und Energie GmbH (HZB)
12489 Berlin, Germany

The ORCID identification number(s) for the author(s) of this article can be found under https://doi.org/10.1002/aenm.202403811

[+]Present address: Department of Physics, Chalmers University of Technology, Gothenburg SE 412 96, Sweden

[++]Present address: Institut Lavoisier de Versailles (ILV), University of Versailles Saint Quentin en Yvelines (UVSQ), Versailles 78000, France

DOI: 10.1002/aenm.202403811

ethylene carbonate and linear carbonates at the K-metal surface was found to lead to soluble dicarbonates (dialkyl dioxahexane dioates) species[14,15] in a significant amount (even under open circuit voltage (OCV) conditions)[11,13] that diffuse to the positive electrode (e.g., Prussian whites) and induce side reactions and self-discharge.[16,17] Because the reactivity of alkali metals toward electrolyte components decreases considerably from K to Li in line with the periodic law, the graphite electrodes extracted from half cells provide a good approximation for representative picture of the sample surface in lithium systems,[18–20] when the cells are not aged/cycled excessively. Following the conclusions of previous PES studies, the SEI formed in carbonate-based electrolytes on graphite in KIBs is comparatively thick up to the point that the underlying active material cannot be reached by conventional PES. Moreover, such SEI tend to exhibit high contents of organic surface deposits that dissolve readily into the electrolyte.[8,11,21] However, the full cell studies by Hosaka et al.[9] (graphite//$K_2Mn[Fe(CN)_6]$) and Larhrib et al.[22] (graphite//$KVPO_4F_{0.5}O_{0.5}$) provide a different angle to these previous (half cell) results suggesting that in absence of the highly reactive K-metal counter electrode, the SEI layer on graphite is considerably thinner which can be seen from a prominent graphite peak in the C1s photoemission spectra. However, a direct, in-depth analysis has not been performed yet to compare cycled electrode surfaces from half and full cells (with the same materials and under the same testing conditions) at different stages of aging. The recent findings also pose the question, which part of the data obtained from PES experiments on half cells provides valid conclusions for improvements and design principles of KIB full cells and when is utilizing full cells is strictly necessary?

Herein, we aim to address these knowledge gaps by a detailed depth-profiling study from in-house and hard X-ray PES experiments to investigate the differences between the surface layer properties in half and full cell configurations in a carbonate-based electrolyte. Our results demonstrate that photoemission spectra of cycled electrode surfaces are strongly affected by the type of sample preparation chosen (half or full cell), as a result of the SEI layer's altered chemical composition and thickness. From the profound discrepancy in surface layer characteristics between the two sample preparation strategies we conclude that results from half cell samples have to be considered with caution. Our results are particularly relevant in studies that aim to develop a mechanistic understanding of the SEI formation in different electrode and electrolyte environments and the electrolyte development in general.

2. Results

Graphite electrodes for the PES study were prepared in half and full cell configurations using either K-metal or Prussian white $K_2Fe[Fe(CN)_6]$ (KFF) counter electrodes. The electrodes were cycled in a liquid electrolyte mixture consisting of 750 mM KPF_6 in a solvent mixture of ethylene carbonate (EC) and diethylene carbonate (DEC) (EC:DEC, v/v = 1:1). The electrolyte mixture is well motivated as one of the most commonly used formulations currently used in the KIB field, according to a meta study by Hosaka and Komaba.[10] In addition, several previous XPS studies used this electrolyte in their experiments,[11,22,23] thus enabling good comparability between existing work. The EC:DEC solvent mixture is also the basis for a number of revised electrolyte formulations. Investigating the degradation of base components is therefore a relevant subject to understand performance improvements from electrolyte development.

2.1. Electrochemical Results

Figure 1A,B show the specific charge and discharge capacity for the graphite/KFF full cell and graphite/K half cell, respectively. The N/P ratio of the full cell was 1.28, i.e., an excess of graphite was used, which is a common approach to reduce the risk of alkali metal plating[24] and lies in the range of previously used N/P ratios by Larhrib et al.[25] The C.E. and voltage profiles of selected cycles are shown in Figure 1C,D, and F respectively. Half cells showed a stable capacities of around 250 mAh g^{-1} on discharge (deintercalation) over the first 10 cycles. The initial coulombic efficiency (C.E.) was 73.2% and increased to 98.3% in the 10th cycle, which is slightly better than in our previous work[1,26] and in the expected range of reported results by other groups.[2,27] In contrast, the full cell displayer a low initial C.E. of only 53% and consequently a comparatively low initial discharge capacity of 71 mAh g^{-1}. The corresponding charge capacity, related to KFF active material mass in the cell, suggests that the K-inventory in the positive electrode was fully utilized. Nonetheless, the full cell data lies in the expected range of other recent studies that reported values below 70% in similar carbonate-based electrolyte mixtures (Table S2, Supporting Information). It should be stressed that significantly smaller N/P ratios and precycled electrodes are common strategies to boost the capacity and reduce initial losses. For the sample preparation herein, we have refrained from these options. Especially, precycling in a half cell would have created a half cell-like SEI on graphite electrode before it is transferred to the full cell. For the ageing study below, this is not a desirable scenario. The cycling rate changed from C/20 to C/10 after 2 cycles, which was associated with a significant drop in the discharge capacity of around 25 mAh g^{-1}. After 30 cycles the cell retained a capacity of 26 mAh g^{-1}. The capacity retention in a similar range than the data presented in a recent study by Larhrib and Madec[28] who studied graphite/$KVPO_4F_{0.5}O_{0.5}$ full cells in dependence of various N/P ratios in the range from 0.98–1.3. The voltage profile in Figure 1D shows a sloping profile with several steps characteristic to the voltage plateau of KFF at 3.45 and 4.05 V versus K^+/K and, to lesser extent of graphite (profile shown in Figure 1E). In the second and all subsequent cycles, the potential profiles show an increasingly steep gradient with increasing number of cycles and longer constant voltage (CV) sections after reaching the upper voltage limit of 4.15 V. This is a direct result of capacity loss and increasing cell resistance, as seen by the increasing voltage hysteresis in Figure 1D. The graphite/K half cell was cycled for one and ten cycles (the latter is shown in Figure 1B). The graphite electrode achieved specific discharge capacities of approx. 250 mAh g^{-1}, which is close to the theoretical specific capacity of 279 mAh g^{-1} (KC_8). The C.E. (Figure 1C) and specific charge capacities (Figure 1B) over the first three cycles indicate a high degree of irreversible reactions. The excess of K-ion inventory from the K-metal counter electrode compensates for loss of charge inventory. The recurrent electrolyte decomposition below electrode potentials of <1.2-1.5 V[29,30] leads to thick surface layers

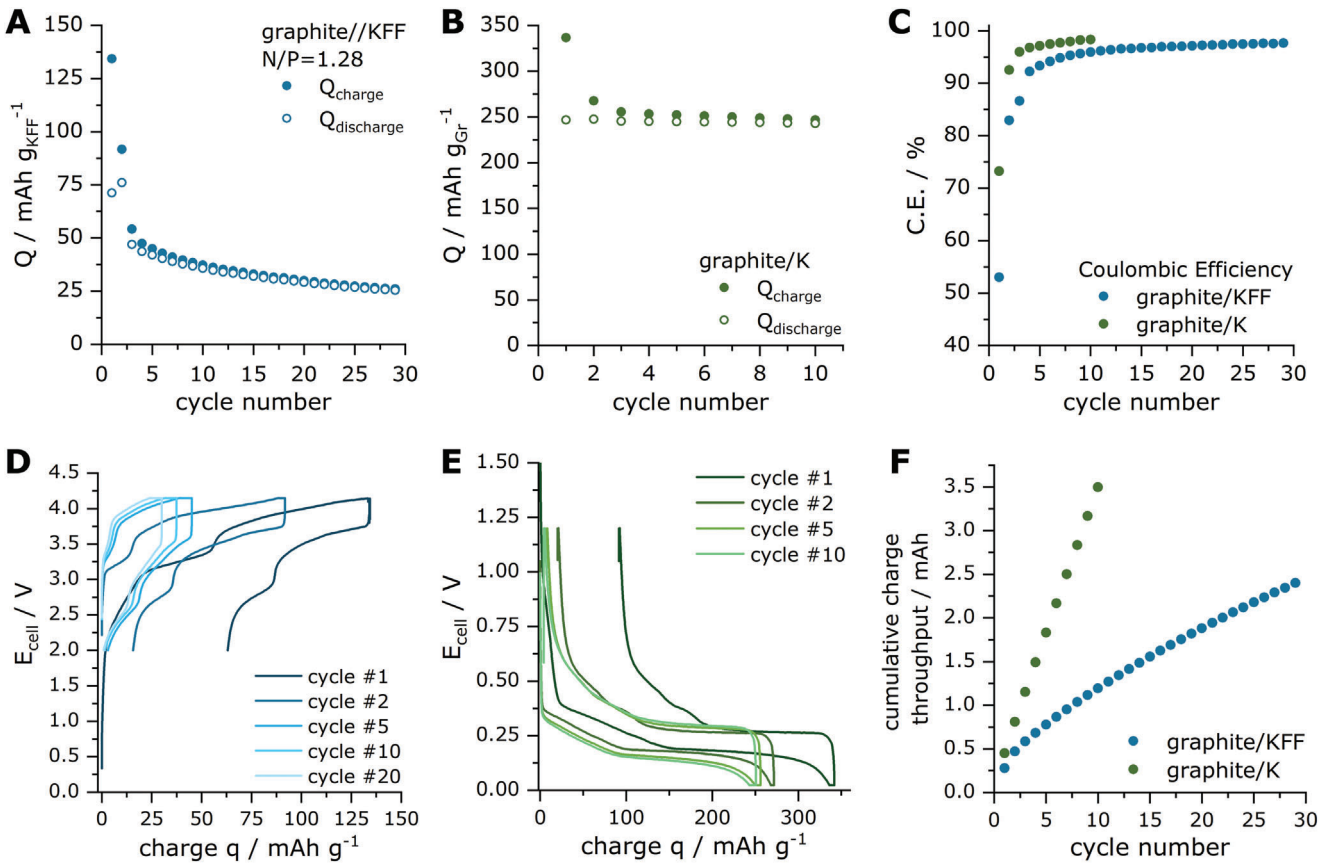

Figure 1. Galvanostatic cycling results of graphite/KFF A) and graphite/K B) and corresponding coulombic efficiencies, C.E. C). The voltage profiles for selected cycles are shown for the full cell D) and half cell in E). The cumulative charge throughput as a function of cycle number is plotted in F. The full cell capacity refers to the active material mass of the positive electrode (in mAh g_{KFF}^{-1}).

and causes gradually increasing overpotentials, as reported previously.[1,11]

Half and full cells performed quite differently, particularly regarding the depth of charge (DoC) that is an important parameter in the SEI layer formation. Therefore, we compared them in this PES study using two different approaches. First, the early ("initial") SEI layer formation on graphite was studied after the first cycle in both cell configurations. Second, we investigated the SEI evolution after continued cycling ("aged SEI"). Because of their different ageing behaviors, we considered it more practical to compare these samples on the basis of their cumulative charge throughput[31,32] instead of a comparison after the same number of cycles. In an attempt to reduce the difference between the charge passed through the half and full cell, the cells were stopped after a different numbers of cycles, i.e., after 10 and 30 cycles respectively. The half cell had reached a cumulative charge throughput of 3.5 mAh while the full cell had reached a cumulative charge throughput of 2.4 mAh. For comparison, if the full cell had been stopped after 10 cycles, the cumulative charge throughput had been only half the value (1.2 mAh, i.e., almost 3 times lower than for the half cell). This affects the SEI layer properties, especially thickness, which scale with the amount of charge passed (and the C.E.). While there will be always discrepancies between two different cell configurations, especially when they perform notably different, using the cumulative charge as sampling criteria helps to align time-dependent (electro)chemical changes in the cell and increases the exposure time of the electrolyte toward critically low or high potentials. As mentioned above, differences may also arise from different DoC, which is an aspect, cumulative charge cannot solve. In full cells with low C.E. the changes in DoC can be quite rapid due to the fast loss of the potassium-ion inventory.

2.2. PES Depth Profiling on Graphite Electrodes

After the cells were stopped in their fully discharged state, i.e., in the deintercalated state for graphite, the electrodes were rinsed immediately after cell disassembly to remove electrolyte salt residues. The electrodes were studied by non-destructive depth profiling using three different photon energies from in-house PES (1487 eV; Al K_α) and synchrotron-based HAXPES (2150 eV and 6450 eV), respectively. Photon energies of 6450 eV allowed measurements of higher binding energy (BE) core levels, specifically K1s (BE ≈ 3607 eV) and P1s (BE ≈ 2152 eV), which have a better photoionization cross section[33] and therefore provide a better signal-to-noise ratio than the corresponding K2s and P2p lines at this excitation energy, while still exhibiting higher kinetic energies. Because of the kinetic energy dependent inelastic mean

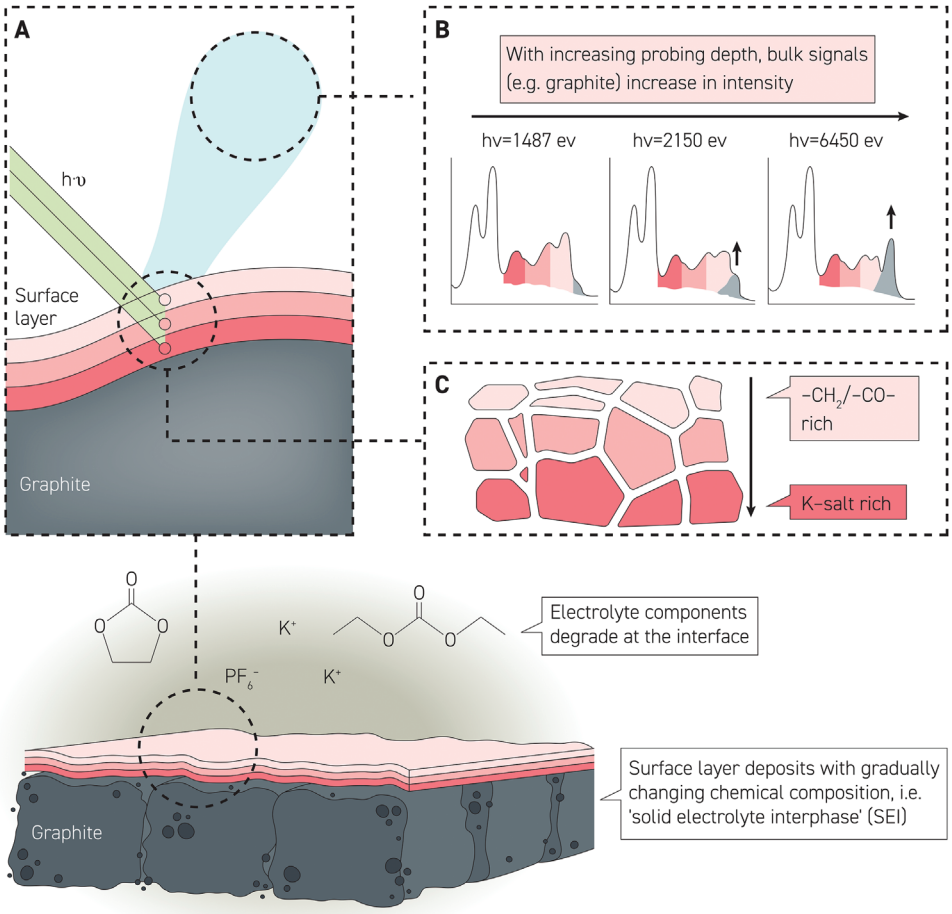

Scheme 1. Graphical summary of the PES depth profiling study: when the probing depth is increased, more information about deeper regions of the SEI and the SEI / (bulk) electrode can be gained. While organic species dominate in the top layers of the SEI, the chemical composition of the SEI is shifting toward more inorganic material in the regions closer to the graphite particles, where for example carbonates are particularly prominent.

free path (IMPF) of the photoelectrons, the probing depth varies both with photon energy and core level (**Scheme 1**). For example, photoelectrons originating from a C1s orbital (BE ≈ 284–292 eV) from an in-house X-ray source (Al Kα ≈ 1487 eV) provide an estimated probing depth of about 7–9 nm (3λ).[34,35] This value increases roughly to about 18 nm (3λ) at a photon energy of 2150 eV and reaches up to 45 nm (3λ) in the case at 6450 eV. Thus, using harder X-rays, the probing volume increases and photoelectrons generated in surface-near regions contribute less to the overall spectrum than at lower probing depths. However, the obtained spectra are always a projection of the photoelectrons emitted from the entire probed volume. In the example in Scheme 1, this is indicated in panel B with a gradual increase of the bulk electrode signal (graphite) marked in grey while the surface features (shades of red) are still present but at decreased relative intensity.

2.3. C1s-K2p Spectra

The C1s spectra of the graphite electrodes from either half or full cells, measured at different photon energies, are shown in **Figure 2** for samples studied after the initial SEI formation after 1 cycle and the after extended ageing (i.e., 10 cycles for half and 30 cycles for full cells), respectively. Survey and core level spectra are provided in the Supporting Information (Figures S1–S4, Tables S3–S6, Supporting Information) for the pristine electrode and from graphite electrodes stored at open circuit voltage ("OCV samples") for the duration of the testing time of the cycled samples (both half and full cells). The spectra consist of a bulk active material signal (sp^2-C, graphite; BE = 283.3±0.1 eV; grey), saturated hydrocarbon species (sp^3-C, -CH-; BE = 285.0 eV; red), ethers/alcohols (-CO-; BE = 286.6±0.1 eV; blue), carboxylates -(C=O)OR; BE = 288.5±0.1 eV green) and carbonates (K_2CO_3 if inorganic, or R_1O-(C=O)-OR_2; if organic in nature; BE = 289.8±0.2 eV; yellow).[8,11,13] The peak assignments above are representative of a variety of structurally similar chemical motives with closely adjacent BEs, stemming from the degradation of electrolyte components into different compounds. The K2p signal is the prominent doublet peak with a characteristic BE distance of +2.8 eV for the $K2p_{3/2}$ and $K2p_{3/2}$ core levels at 292.8+0.2 eV (dark purple) and 295.6+0.2 eV (pale purple), respectively. The peaks can be assigned to K_2CO_3 and potassium salt deposits.[11,13] Because of its proximity to peaks in the high BE C1s region, minor overlaps with carbonates species, e.g. CO_3^-, can be observed.

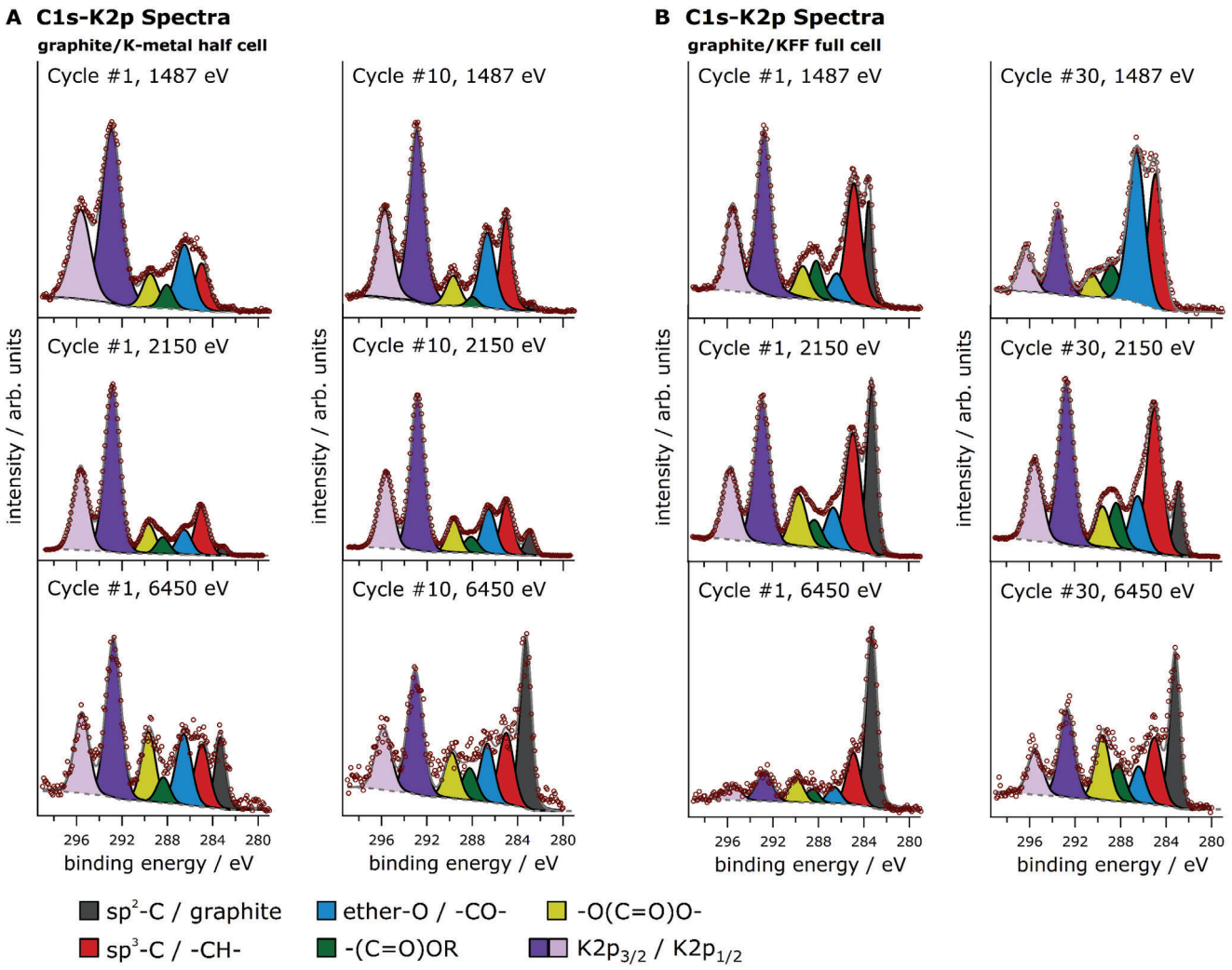

Figure 2. C1s spectra of graphite/K-metal half cell A) and graphite/KFF B) configurations (discharged state) after 1, as well as after 10 (half cell) and 30 (full cell) cycles for three excitation energies (increasing probing depth from top to bottom).

In spectra of samples from half cell configurations (Figure 2A) measured at the lowest probing depth, i.e., the in-house PES spectra, the graphite signal (sp^2-C) is barely visible after only one cycle. This corresponds to a surface layer thickness of around 8–9 nm (from the IMFP of photoelectrons excited with 1487 eV). In the corresponding HAXPES spectra measured at 2150 eV, the graphite signals gained moderately, yet notably, in intensity. By increasing the probing depth further using 6450 eV excitation energy, the bulk graphite peak becomes the most prominent C1s feature in the spectrum of the electrode after 10 cycles. Interestingly, in all spectra after 10 cycles, the sp^2-C peak displays larger peak intensities, which suggests somewhat counterintuitively that the surface layer thickness has decreased from the 1st to the 10th cycle (for a more detailed discussion, see below).

After the first cycle in the half cell (Figure 2A, *Cycle #1*) the graphite surface shows an intense -CO- component in both the in-house and the HAXPES (6450 eV) spectra. Only at 2150 eV is the -CO- peak intensity notably lower. In samples aged for ten cycles, the relative intensities between the sp^3-C/-CH- peak and -CO- peak remain almost constant, with a slightly more intense saturated hydrocarbon signal. Their intensities with respect to other signals decrease with probing depth, indicating that both components display higher contents in the outer SEI, i.e., the surface-near region. With increasing probing depth, higher intensities are observed for both the carbonate peak and carboxylate peak. At 6450 eV the intensity of the carbonate peak approaches that of the sp^3-C and -CO- peaks, indicating higher contents of this component in the inner SEI, i.e., the deeper subsurface/near-bulk regions. This is in general agreement with the literature that SEI regions close to or in contact with the active material show higher inorganic content,[20,36,37] which derives from organic compounds, such as ethylene dicarbonate salts ($(CH_2\text{-}OCO_2K)_2$), via subsequent reactions.[15,38]

A comparison of the graphite bulk peak (sp^2-C) in the spectra of full cell samples (Figure 2B) with those from half cell experiments shows significant differences in the development of the SEI layer thickness after 1 and 30 cycles. After 1 cycle, the graphite signal is prominent in all spectra and its relative peak

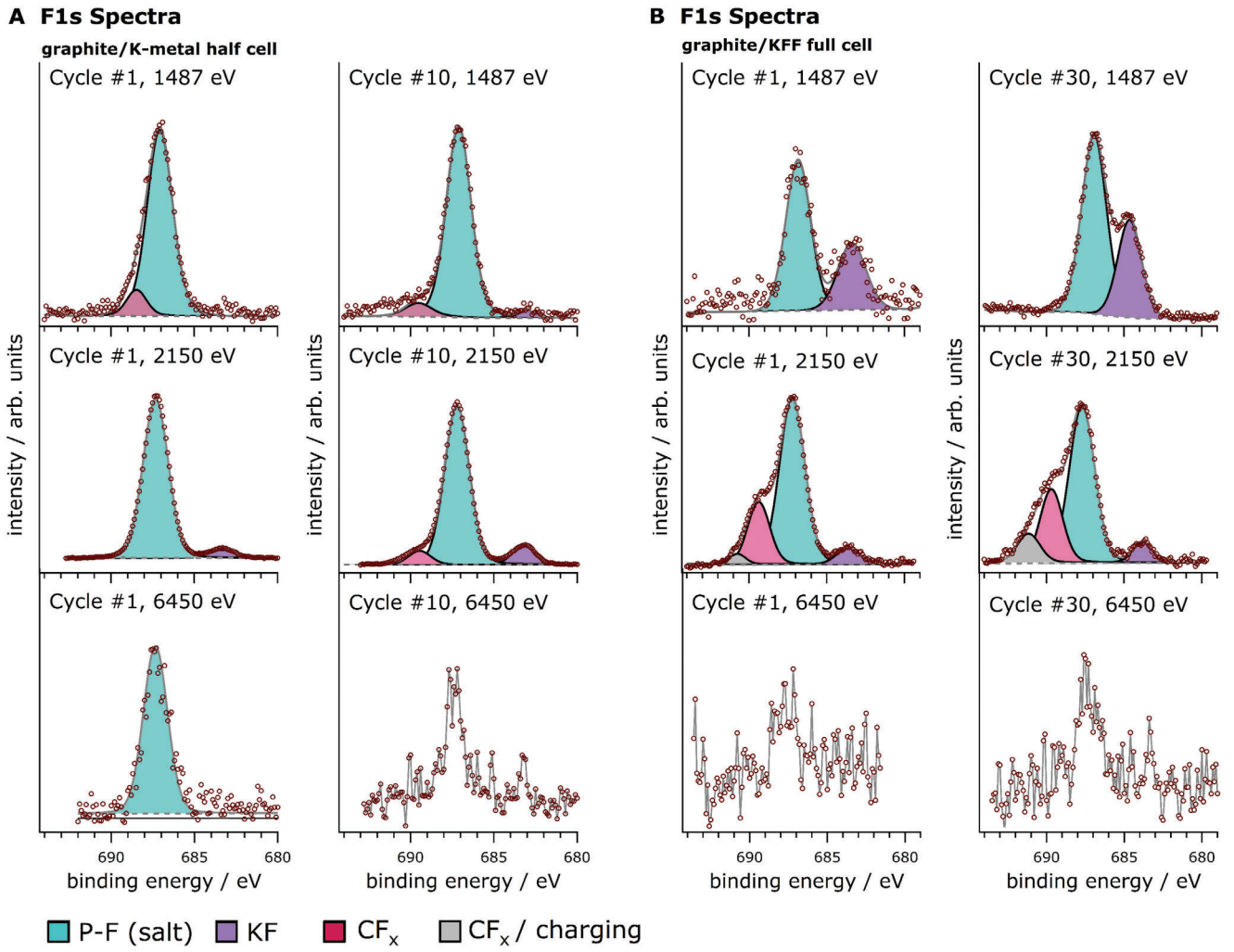

Figure 3. F1s spectra of graphite/K-metal half cell A) and graphite/KFF B) configurations (discharged state) after 1, as well as after 10 (half cell) and 30 (full cell) cycles for three excitation energies (increasing probing depth from top to bottom).

intensity increases with increasing photon energy. However, after 30 cycles, the peak is strongly attenuated relative to the other signals and disappeared entirely in the in-house spectrum, indicating a considerable increase in the SEI layer thickness with increasing cycle number. The SEI composition shows distinct differences from the surface layer compositions formed in half cells. Apart from the in-house spectrum after 30 cycles, the sp^3-C/-CH- peaks are more distinct from the rest of the signals attributed to SEI components. While the K2p peaks in half cell samples show measurably higher intensities relative to SEI components in the C1s spectra, their intensity is consistently lower in spectra of the full cell samples, which indicates lower amounts of potassium salts. From the decreasing intensities of both the -CO- and -(C=O)OR peak and the gradual increase of the carbonate peak with increasing probing depth, it can be concluded that the former species have higher concentrations in the uppermost layers of the SEI (outer SEI), while the concentration of the latter is higher near the bulk electrode (as also observed in half cells as well).

2.4. F1s Spectra

Apart from the C1s spectra, the most significant differences in the surface layer composition between half and full cells are observed in the F1s spectra, shown in **Figure 3**. The KF (purple) is found at 683.3±0.1 eV, and a prominent P-F peak (teal) is observed at 687.3±0.1 eV (mostly KPF_6) in accordance with previously reported reference measurements.[11,13] A peak at 689.4±0.1 eV is assigned to organic fluorinated compounds R-CF_x (pale red).[11,39] In addition, some spectra show a fourth component (grey) at around 690.8±0.1 eV that could not be further assigned. The signal might originate from differential charging effects of an insulating fraction of salt residues, because even for highly fluorinated compounds, such as Teflon $(C_2F_4)_n$, BEs larger than 690 eV are rarely reported.[40]

The half cell data (Figure 3A) shows mainly a P-F peak with minor amounts of organic fluorinated compounds at higher BEs, as well as small amounts of KF at lower BEs, which is in good agreement with our previous in-house measurements.[11] The

signal-to-noise ratio of spectra measured at 6450 eV was relatively high because of the decaying photoionization cross-section of atoms with increasing excitation energy.[41] From the first to the tenth cycles, the P-F peak intensity decreased significantly, which is likely a result of a thicker surface layer with an overall lower fluorine content. In the in-house and 6450 eV spectra after 1 cycle, only a faint KF signal can be seen, which was not explicitly fitted. The KF content increased relative to the P-F peak at higher probing depths in the spectra obtained at 2150 eV and also from the first to the tenth cycle. This result suggests that KF accumulates during cycling in the SEI layer either through recurrent electrolyte salt degradation or proceeding degradation reactions of deposited material (e.g., known from LIBs, ref.[42]) Moreover, KF is a component found in higher concentrations in the inner SEI.

In contrast, the F1s spectra of full cell samples (Figure 3B) differ distinctly from those of half cells. It can be observed that the relative intensities of the KF peak are notably higher relative to the P-F signal in the in-house spectra. This could indicate higher KF contents or significantly lower KPF_6 (P-F) contents in the outer SEI layers. However, it should be emphasized that the noisy F1s spectrum after one cycle is particularly indicative of low overall fluorine contents after initial SEI formation.

Samples measured at 2150 eV showed relative peak intensities more comparable to those of half cell samples. While the relative peak intensity of KF increased in the in-house spectra from the first to the tenth cycle, it remained approximately constant in the spectra measured at 2150 eV. This is also an indication that the surface layer was not fully penetrated in the in-house measurement, due to the lower IMPF of the F1s photoelectrons. In addition, a major difference in the latter spectra is the presence of a more prominent peak of fluorinated organic compounds, as well as the aforementioned fourth component at an even higher BE. Both features increase with respect to the P-F peak from the spectrum after cycle 1 to that of cycle 30.

A relative peak shift of the P-F and KF components between the in-house and synchrotron data was observed for the sample after 30 cycles (Figure 3B). Specifically, the P-F and KF peaks moved closer together by 1.6 eV (from a peak distance of 3.7-4.0 eV, in agreement with ref,[11,13] to 2.4 eV) in the in-house spectrum, which correlates with a corresponding relative shift between the P-F (PF_6^-) peaks of the in-house and 2150 eV spectra (full cell, cycle #30) in **Figure** 4C. Although the origin remains unclear, the increase of relative shifts might be explained by increase of differential charging through combination of 1) the insulating nature of KPF_6 and KF deposits in the SEI, 2) the increasing thickness of the surface layer and thus differential charging effects.[11]

2.5. P2p and P1s Spectra

For the analysis of phosphorus species, the P2p core levels were recorded in experiments with 1487 eV and 2150 eV, respectively. Because of the low photoionization cross-section of the P2p orbital at 6450 eV, the P1s orbital was used instead at this photon energy. P2p spectra show characteristic doublet peaks for the $P2p_{3/2}$ and $P2p_{1/2}$ core levels with a BE distance of 0.9 eV (intensity ratio 2:1) due to spin-orbit splitting.

The P2p spectra of graphite electrodes from half cell configurations show a distinct PF_6^- doublet (teal green) and additionally $PF_x(OR)_y$ components in HAXPES spectra at both probing depths.[20,37] The intensity of the $PF_x(OR)_y$ species is relatively small compared to the PF_6^- peak. Salt degradation appears to occur throughout the first ten cycles, leading to the accumulation of products such as $PF_x(OR)_y$ (and KF) in the SEI.

Similar to the F1s spectra, signal intensities (and therefore P contents) were generally lower in the surface layers of full cell samples. A curve fit was applied on all spectra, but due to the high noise level, only the peak assigned to PF_6^- (teal green) is clearly discernible. Therefore, the $PF_x(OR)_y$ component was not included in the fit of the spectra recorded at 2150 eV. Both species could be clearly distinguished in the 2150 eV sample after 10 cycles. The relative intensity of the $PF_x(OR)_y$ degradation product increases with the number of cycles, thus correlating $PF_x(OR)_y$ and KF formation in the P2p and F1s spectra. The P1s spectra at 6450 eV show only one peak at 2152 eV, which is assigned to the PF_6^- anion.[37]

2.6. Other Core Levels

Besides the above-discussed elements, spectra of the O1s, K2s (1487 eV & 2150 eV) and K1s (6450 eV) environments are provided in the supporting information (Figures S1,S2, Supporting Information). The K2s and K1s spectra (Figure S2, Supporting Information) show a single peak for the potassium salts formed during SEI formation. O1s spectra were fitted with two components: a carbonate/carboxylate peak (dark yellow) at about 531.3±0.2 eV and an ether peak (-CO-, blue) at 533.3±0.2 eV. In the case of the in-house spectra, the Na KLL Auger line is observed after the first cycle. Na-ions are introduced into the system due to the CMC-Na binder of the graphite electrodes. After ten cycles, the Na^+ content in the SEI layer is probably below the detection limit. As Auger peak positions in BE scale are a function of photon energy, the Na KLL signal in the O1s spectra at 2150 eV and 6450 eV is no longer observed. In accordance with the C1s spectra, it was found that in O1s the -CO- peak increases with cycle number. Its relative peak intensity decreased with increasing probing depth with respect to the carbonate/carboxylate peak. the Na KLL signal in the O1s spectra at 2150 eV and 6450 eV is no longer observed.

2.7. Surface Composition Analysis

From the peak areas of the fitted photoemission spectra discussed above, the atomic concentrations can be derived using relative sensitivity factors (RSF). RSF values for the HAXPES data were determined as described in equation 1 and are summarized in Table S1, Supporting Information). Quantification of in-house data is performed in the analysis software Avantage based on a RSF library (see Experimental Section). The bar plots in **Figure** 5 provide a brief overview of the elemental distribution (values provided in Tables S3–S6, Supporting Information) and the dominant chemical species in the SEI layer of graphite cycled in different cell configurations, and outline the surface layer evolution by comparison of the atomic concentrations after one initial cycle,

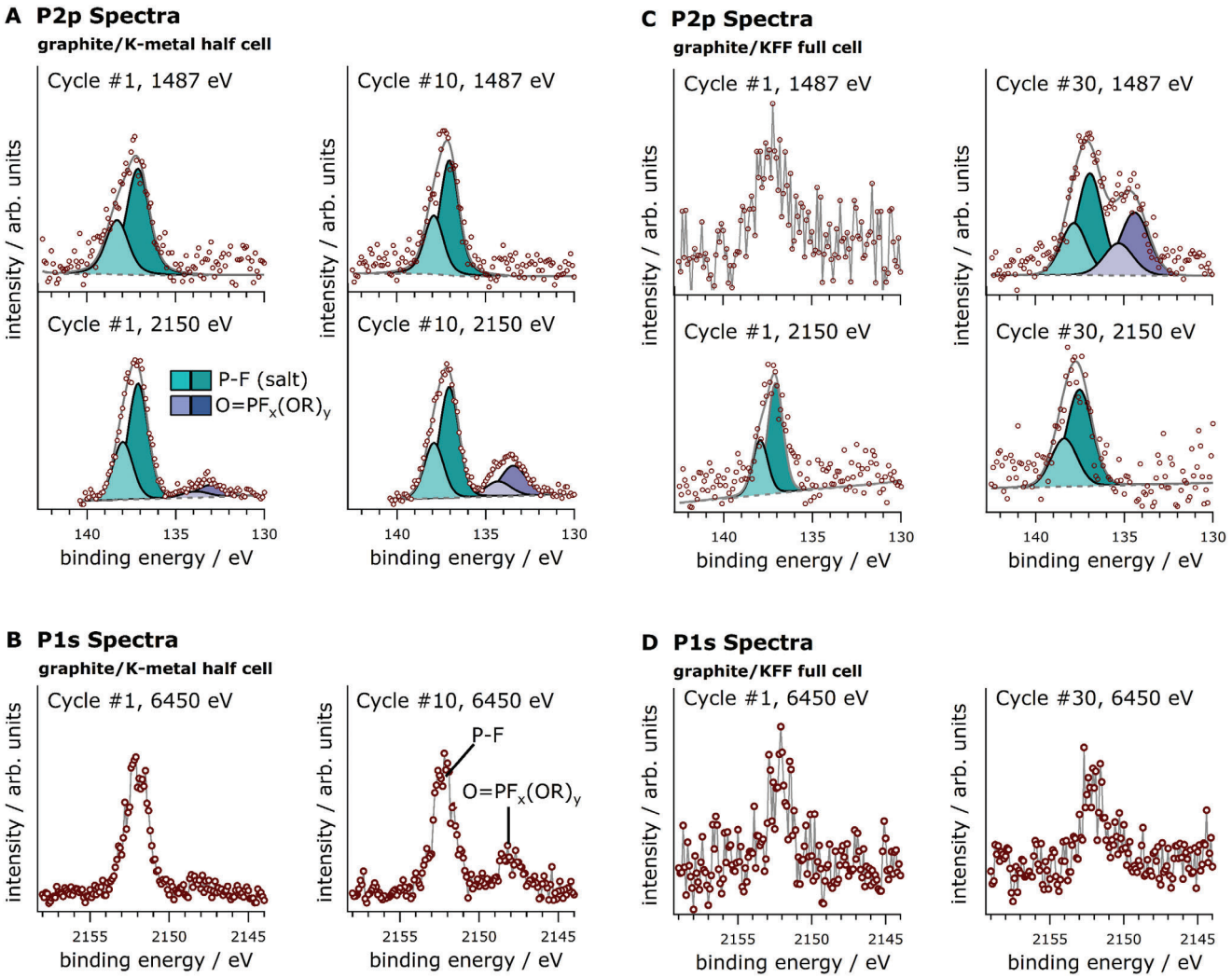

Figure 4. P2p and P1s spectra of graphite/K-metal half cell A & B) and graphite/KFF C & D) configurations (discharged state) after 1, as well as after 10 (half cell) and 30 (full cell) cycles for three excitation energies (increasing probing depth from top to bottom).

as well as after 10 (half cell) and 30 (full cell) cycles, respectively. In general, the quantification of photoemission spectra is associated with a comparatively large margin of error in the range of up to several at.%, which is due to uncertainties related to the respective curve fits (peak widths and positions) of strongly overlapping signals (e.g., O1s spectra). IMPF-corrected RSF values are further based on the assumption of a homogenous surface layer, which is not the case for SEI layers. The atomic concentrations derived recently by Allgayer et al.[11] for graphite-K half cells (stopped after 2 initial cycles; in-house XPS) are in good agreement with the surface layer contents found herein for the half cell sample after 1 cycle within a margin of <3–4 at.% (except for the P-F and C = O).

Key findings of the quantification in Figure 5 are a larger fraction of P-F species in the SEI of half cells and in both cell types overall low content of KF, compared to corresponding Li cells.[11] Moreover, the KF content in full cells was generally even lower than in the half cell samples. Given the small fraction of alkyl fluorophosphates (Figure 4), it can be concluded that the P-F contribution originates mainly from PF_6^- that deposited at the electrode surface or was trapped in the thick SEI layer formed in half cells. The oxygen content in this comparison is notably larger in full cells and is likely a result of the formation of polymeric or inorganic carbonate species and carboxylates that form during electrode degradation. The sum of C1s and O1s species in full cells makes up more than 70 at.% of the overall surface layer. However, this includes a notable fraction of the bulk graphite signal (sp^2-C). Because of the thinner surface layers, the contribution of this signal is larger in full cell samples. In contrast, in half cells the total C1s and O1s content varies in the range between 50–75 at.%. At lower probing depth (in-house data), the C1s+O1s content is higher than in the data acquired at 2150 eV, which is indicative of a composition gradient when switching between different probing depths. The potassium content in full cells after one cycle is generally smaller than in half cells. The potassium content determined from HAXPES measurements is larger, which is likely due to the fact of the higher probing depth, which can have an impact on the relative fractions when a

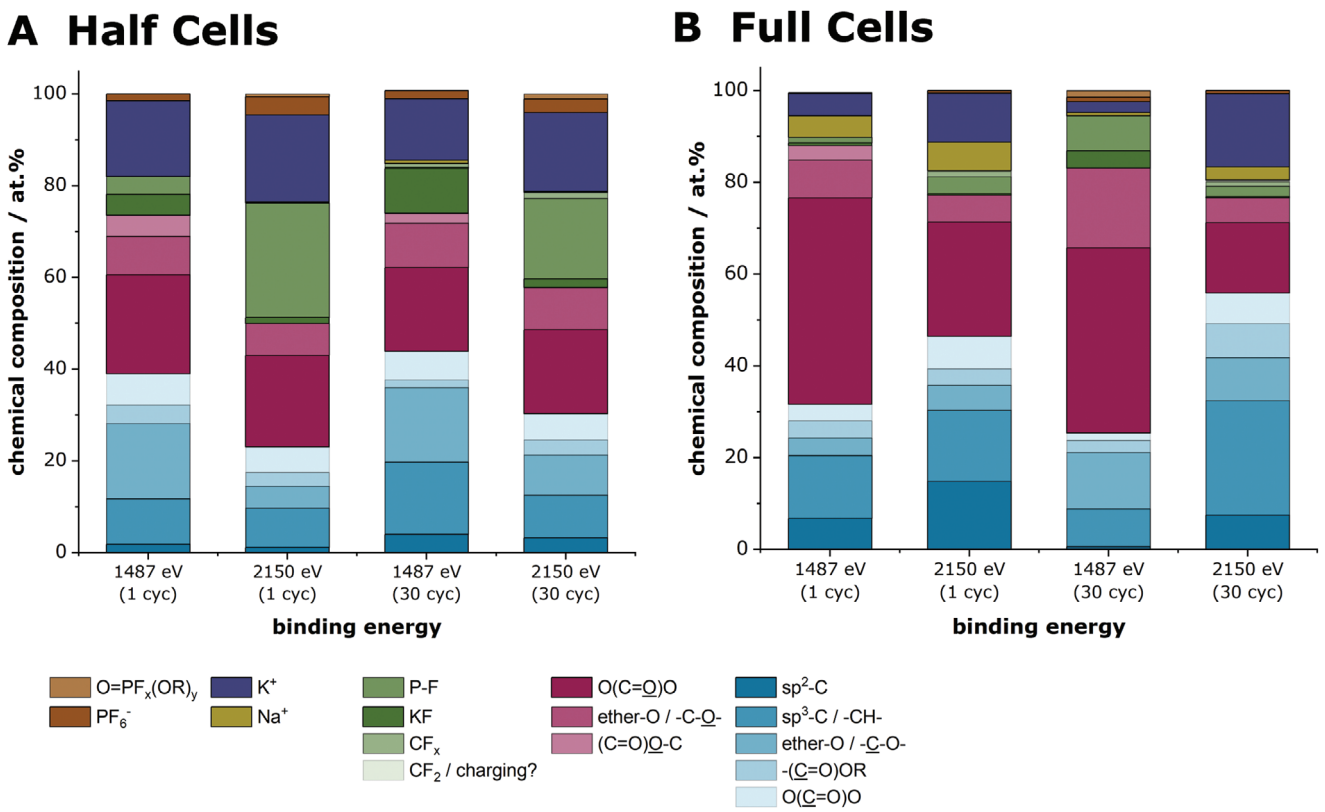

Figure 5. Surface composition analysis derived from in-house (1487 eV) and HAXPES (2150 eV) spectra recorded for graphite electrodes cycled in half and full cells.

chemical gradient is present (IMPF dependency of the respective photoemission spectra). There is a notable increase in the K-content in the HAXPES data (2150 eV) of full cell samples from one to 30 cycles, which is generally smaller than in aged half cell samples. As previously mentioned (Figure 2), the SEI layer on graphite in full cells grows continuously, while in half cells a dissolution appears to take place. This is seen in Figure 5 quite clearly by the higher sp^2-C content in half cells after 10 cycles, compared to the sample cycled for only one cycle. In contrast, the sp^2-C content in full cells decreases with increasing aging duration.

3. Discussion

The formation of stable SEI layers on graphite electrodes is a key challenge for KIBs with higher capacity retention, higher energy efficiency and longer cycle life. Photoelectron spectroscopy plays a major role in determining surface layer composition and thickness during its evolution, as a highly surface sensitive technique. Previous studies reported XPS and PES results after different testing conditions and aging states. For example, Larhrib et al. investigate the SEI formed in their graphite/$KVPO_4F_{0.5}O_{0.5}$ cells[22] after 50 cycles, while Hosaka et al. aged their graphite/$K_2Mn[Fe(CN)_6]$[9] full cells for 10 cycles. Therefore, it was one aim in this study to compare graphite surfaces of half and full cell configurations under similar testing conditions and follow the SEI evolution by investigating the initial SEI formation after 1 cycle and after short-term cycle-aging. The resulting SEI layers were investigated by a PES depth profiling approach, leveraging different probing depths by variation of the excitation energy (Scheme 1).

3.1. Graphite SEI (Half Cells)

It was demonstrated that a heterogeneous surface layer was formed that displayed an organic-inorganic gradient with more organic species in the outer regions, i.e., toward the electrolyte phase, and more inorganic species in the inner regions, i.e., closer to the electrode surface. This finding is in general agreement with previous PES literature and appears to be valid across different monovalent cell systems.[8,18,43,44] By studying the SEI compositions and thicknesses, as well as ageing behavior, it was possible to identify the main differences between the surface layers formed on graphite electrodes with two different cell configurations, which were most pronounced in the respective C1s and F1s spectra.

In half cell setups, the graphite signal in the C1s spectra was more intense (relative to other signals) at any probing depth for the samples exposed to the longer cycle-ageing experiment. This result suggests that after the initial SEI formation in the first cycle, the surface layer became thinner as cycling continued. In other words, the SEI layer is quite dynamic at this early stage of cycling and components may dissolve over time. This is

consistent with the high contents of ether species (-CO-) on the surface, which is notably elevated compared to SEI layers formed during intercalation of Li^+ into graphite.[11,20,45] Their solubility is generally higher in the electrolyte, and therefore gel-like layers are more likely. As a result, the SEI layer could be more permeable to electrolyte components and thus promoting recurrent irreversible reactions, resulting in low coulombic efficiency.

Our results are in good agreement with previous XPS/PES studies on graphite/K half cells investigated under OCV storage conditions[11,12,15] or over the first few cycles.[8,11] Specifically, the high organic contents of the SEI layers in half cell configurations and the rapid surface layer growth are markedly different characteristics to corresponding Li-systems. Particularly the low contents of fluorides could play a role in the poorer passivation properties.[11] These studies highlighted that thick SEI layers form after only one galvanostatic cycle.[8] Notable surface changes are also rapidly observed under OCV storage (even prior to any cycling) over just a couple of days.[12] The formation of considerable amounts of -CO- species is a central difference to the SEI layers in LIBs. -CO- species include not only ethers but also alkoxides (ROK), which originate from the concerted degradation of ethylene carbonate (EC) and linear dialkyl carbonates (e.g., DEC) and are formed in the presence of any alkali metal.[12,15,46–48] Their rate of formation is strongly dependent on the alkali and is greatly accelerated in case of potassium.[14] The ethylene bis(alkyl dicarbonate) formation is a source for continued degradation reactions by repeated nucleophilic attacks of alkoxides, generating oligomeric products and more alkoxides amongst others, as previously reported by Gachot et al. for both Li[49] and K cells.[15] Another possible pathway is the autocatalytic degradation of carbonates by fluorophosphates (from the hydrolysis of PF_6^-).[50,51] However, the P2p and F1s spectra in this study suggest that their formation is considerably less than in SEI layers of Li-containing electrolytes (see below).

3.2. Graphite SEI (Full Cells)

Samples from full cells showed the more intuitive behavior of a gradually growing SEI. After the first cycle a prominent graphite peak could still be observed even at the lowest probing depth, highlighting the fact that the SEI formed in the full cell environment is considerably thinner. Higher porosity and a more heterogeneous SEI density could also play a role, since the deposition process and the type of degradation products formed are likely affected by the limited charge carrier inventory and a rapidly decreasing depth of charge/discharge (i.e., a less reducing environment). The -CO- content is initially lower in the surface layer but builds up as ageing progresses. Similarly, organic fluorinated species also appear to accumulate only gradually in the surface layer, which is in stark contrast to the elemental distribution in half cells. In agreement with our previous study,[11] the LiF content in Li half cells was as high as 10 at.%, while the corresponding K-cells showed only low KF contents of a few at.% (after initial SEI formation). From the elemental distribution (Figure 5), it can be stated that the relative peak intensities in the F1s spectra show that the KF content and in fact the fluorine content overall remain minor components in surface layers of full cells. The P2p spectra are in good agreement with this finding, suggesting that electrolyte salt degradation, the source of fluoride formation, occurs at a low level. This is particularly true when compared to the corresponding spectra obtained in Li cells.[11,20] The low tendency for salt degradation and KF formation, together with the overall thinner surface layer, is also reflected in lower relative K contents (Figure 5).

Recent PES results on KIB full cell configurations, i.e., graphite/$KVPO_4F_{0.5}O_{0.5}$ cells[22] and graphite/$K_2Mn[Fe(CN)_6]$[9] further highlight considerably thinner SEI layers and low K-salt contents, which is indicated in the relative peak intensities between characteristic SEI signals and the K2p doublet. Our findings confirm these previous general trends, particularly in terms of low KF contents that appear to play an important role in the passivation quality of the surface layer. These differences become most apparent when comparing the SEI layer composition to LIBs, like graphite/$LiFePO_4$ full cells, that displayed carbon contents of less than 25% and LiF making up more than 60%[20] after 9 cycles. Beyond the comparison to SEI characteristics found in half cells, our study contributed with additional information on the initial SEI layer formation (after 1 cycle) and allowed us to establish compositional changes to cycle-aged electrodes.

3.3. KFF Surface Layer (Full Cell)

The spectra of the KFF electrode were only briefly discussed, as the main focus was placed on development of the SEI layer formation and evolution on graphite. A detailed surface analysis is provided in the Supporting Information (Figures S7–S9, Supporting Information). Briefly, our analysis showed a high level of complexity in the photoemission spectra due to the strong overlap of different components in the C1s spectra. For instance, the contribution of hydrocarbon species (-CH-) from electrolyte degradation reactions is no distinct feature in the C1s spectrum and contributes to the peak intensities of the C≡N and carbon black signals around 285.3 eV. However, its contribution can be seen indirectly in the comparison between electrodes analyzed after one and 30 cycles. The attenuation of the bulk carbon black signal is an indication of a comparatively slow but gradual increase of a surface layer. The practical capacity of KFF was accessed fully on the first cycle, but a large fraction of the charge carrier inventory was lost to side reactions on the first cycle (see voltage profiles, Figure 1D). Despite this considerable loss of K-ions over just a few cycles, there were comparatively little changes observed at the electrode surfaces of samples stopped after the first and the 30th cycle, respectively.

3.4. Summary

This study bridges the gap between previous PES analyses addressing the initial SEI formation and those addressing aged electrodes from longer cycling intervals, by investigating SEI characteristics of graphite electrodes from both ageing time scales. Because of different material choices and ageing conditions in previous studies direct comparisons of PES results are challenging. This issue was addressed herein by preparing half and full cell samples from the same materials and under the same testing conditions, thus allowing a most direct comparison between the two cell configurations. Our findings relate not only

to configuration-dependent changes in surface layer composition and thickness but also shed light on the further SEI evolution over prolonged cycling. This is reflected in the comparison of the SEI layer properties after two different charge throughputs, where a significant SEI dissolution was observed between the 1st and 10th cycle on graphite electrodes from half cells, whereas the SEI formed on graphite in full cells showed a continuous growth from the 1st to the 30th cycle. SEI layers on graphite surfaces from full cells turned out to be significantly thinner than corresponding surfaces from half cells. This observation is in agreement with a recent studies by Larhrib et al. (graphite/$KVPO_4F_{0.5}O_{0.5}$),[22] and in stark contrast to the SEI layer properties of the half cells shown herein and to a previous PES study by Naylor et al.[8] (SEI layer changes during the first formation cycle). The underlying cause for both observations is the extensive electrolyte degradation of carbonate-based solvent mixtures comprising of EC and a linear carbonate at the K-metal electrode and associated crosstalk processes induced by a critical accumulation of degraded species with high solubility in the solvent/electrolyte mixture. The soluble degradation products travel and deposit on other cell components, including the WE.[14,15] Therefore, the SEI composition observed in half cells is likely to include a considerable proportion of surface deposits originating from the K-metal counter electrode, as confirmed in storage tests in several studies.[11–13] Ultimately, the change in surface properties in different cell configurations may challenge what reliable information can be obtained from half cell testing.

3.5. Limitations

In this study we used the most commonly used carbonate-based electrolyte formulation, i.e., KPF_6 in EC:DEC, according to Hosaka and Komaba.[10] Based on previous findings, similar results are expected for other carbonate-based solvent combinations, e.g. EC:DMC or EC:EMC, where analogue soluble degradation products were found to accumulate in the electrolyte in contact with potassium metal.[14,15] In recent years, more diversification into other solvent classes is seen, for instance electrolyte mixtures based on trietyl phosphate (TEP) in combination with high concentrations of KFSI,[52,53] which consequently shows different passivation and degradation behaviors and mechanisms. PES is an ex situ method and as pointed out in the experimental section, electrodes are washed with DMC prior to analysis. Inevitably, low-molecular degradation products are likely removed in this process from pores or the surface. The surface that is observed with PES hence includes the insoluble fraction of the SEI. Additional microscopy and spectroscopy techniques can therefore contribute to a more holistic picture of the SEI layer properties over various length scales.[54]

4. Conclusion

With this study, we aimed to highlight the differences between surface layers formed on graphite electrodes in half cell and full cell K-ion configurations. In the KIB field the necessity of detailed knowledge of the sensible influencing factors in different cell configurations, as well as good judgement on their respective limitations, appears to be strongly amplified in comparison to more "forgiving" Li-based setups. The SEI layers that are formed on graphite electrodes in either half or full cell configurations display notable discrepancy with respect to chemical composition, thickness and in their ageing behavior. Hence, data from half cell samples might be misleading, if a thicker SEI layer is the result of pronounced crosstalk of degradation products formed at the potassium metal counter electrode. Their deposition and subsequent reaction at the working electrode led to altered chemical compositions that reflect the SEI composition of a full cell only poorly. Moreover, faster capacity fade and shallower depth of charge in a full cell might complicate a comparison by cells stopped after the same number of cycles and (cumulative) charge throughput might become a fairer basis of comparison. Although more material testing in full cell configurations would be desirable, there are additional issues associated with full cell experiments, starting from a reliable, ideally commercial, material basis (material availability gap) to produce reproducible electrode coatings and defined loadings.[55]

In the light of recent diversification in electrolyte formulations,[52,56–58] there are ample opportunities for in-depth studies on SEI evolution in other solvents and salts, e.g. ethers in combination of TFSI- or FSI-based salts.[59] Furthermore, our results motivate to revisit and critically challenge established test procedures for half cell configurations. This includes the value of rate-capability tests of electrodes that grow much thicker surface layers in half cells than in full cells. Another example are electrolyte (additive) screenings and related mechanistic studies, due to extensive reactions at the K-metal counter electrode and the resulting interferences of these reaction products at the working electrode through deposition and successive reactions.[60]

In a broader context, the analysis of cell setups made from standard materials (e.g., carbonate-based electrolyte mixtures) promote the comparability of results between different cell chemistries and thus make an impact in identifying underlying chemical trends, for example the reactivity series amongst the alkali metals in organic electrolytes[61] or the solubility of alkali metal salts and their role in the formation of protective SEI layers.[62]

5. Experimental Section

Materials: All materials were used as received, unless stated differently. Potassium metal (in ampules; Alfa Aesar, 99.95% trance metal basis) opened and stored in an Ar-filled glovebox (MBraun, $H_2O < 0.1$ ppm, $O_2 < 0.1$ ppm). C-NERGY KS15L graphite (d90 = 17.2 µm; BET = 20m^2 g^{-1}) and SUPER C65 carbon black was kindly provided by Imerys Graphite & Carbon. $FeSO_4 \cdot 7\ H_2O$ (ACS reagent, >99.0%), $K_4Fe(CN)_6 \cdot 3\ H_2O$ (>98.5%), poly(vinylpyrrolidone) (PVP, M_w = 40 kg mol^{-1}) and sodium citrate tribasic dehydrate (>99.5%) for the prussian white synthesis, sodium carboxymethyl cellulose (CMC-Na) and polyacrylic acid (PAA, M_v = 1.250 kg mol^{-1}) binder, potassium hexafluorophosphate (KPF_6, ACS reagent, >99.0%) and N-methyl pyrrolidone (ACS reagent, >99.0%) were purchased from Merck. Ethylene carbonate (EC, >99.0%) and diethyl carbonate (DEC, >99.0%) were acquired from BASF. Poly(vinylidene difluoride) (PVdF, Kynar HSV900, Arkema) was obtained from Arkema. Coin cells from steel-grade SUS316L and SUS304 were purchased from Hosen and MTI, respectively. Whatman glassfiber separators (GF/D) and Celgard 2325 trilayer microporous membranes (PP/PE/PP) were cut into discs of 16 mm in diameter. In addition, glassfiber separators were dried at 120 °C

overnight under vacuum and transferred directly without air exposure into an Ar-filled glovebox.

Synthesis $K_2Fe[Fe(CN)_6]$ (KFF): Potassium iron hexacyanoferrate ($K_2Fe[Fe(CN)_6]$, KFF) was prepared by a co-precipitation method from an aqueous solution of $FeSO_4$ and $K_4Fe(CN)_6$, yielding a chemical composition of $K_{1.90}Fe[Fe(CN)_6]\times 1.0H_2O$ (from thermogravimetric analysis and inductive coupled plasma optical emission spectroscopy) as reported previously.[4,63,64]

Electrode Preparation: Slurry preparations were conducted under ambient conditions. Slurries were prepared using a planetary mixer (Thinky, ARV-310P). The binder solutions for the positive electrode was prepared prior to slurry preparation, a 10 wt.% PVdF solution in NMP. The solution was stirred at room temperature overnight to allow the polymers to dissolve. The resulting electrode coatings were dried under reduced pressure in a glass oven (Büchi, Switzerland) to enable sample transfer without further air exposure after the drying step.

KFF Electrode Preparation: Electrode slurries were prepared containing 180 mg of KFF, 90.0 mg of carbon black (CB), 30.0 mg of PVdF, (overall electrode composition 80:10:10 ratio by mass, wt.%). Electrode coatings were produced by doctor blading and dried subsequently in a vented temperature chamber at 60 °C overnight to remove NMP. The electrode sheets were cut into discs with a diameter of 16 mm and a mass loading of ≈1 mg cm^{-2}. The electrode discs were then dried at 110 °C for 12 h under vacuum (10^{-3} mbar) and transferred to an Ar-filled glovebox.

Graphite Electrode Preparation: Graphite electrodes comprised of 95 wt.% KS15L graphite, Super C65, and a CMC-Na:PAA binder mixture in a weight ratio 95:1:2:2. The binder solution was prepared by dissolving 20 mg of CMC-Na and 20 mg of PAA in 2 mL deionized water using a Thinky Mixer (200 rpm for 5–10 min). Then 20 mg of Super C65 powder was added and mixed to a slurry for 5 min at 2000 rpm. A total of 1.9 g KS15L was added in two batches to the slurry and after each addition the suspension was mixed for another 5 min at 2000 rpm. More deionized water was added as necessary to achieve a suitable viscosity for coating (ca. 4.5 mL H_2O in total). The slurry was coated on copper foil (Goodfellow, 0.01 mm, 99,9%) with a doctor blade with a small slit size (d = 60–80 µm;, i.e., d > KS15L particle size) to produce thin electrodes to match the KFF electrode loadings. The electrode coating was dried overnight under ambient conditions. Then, electrode discs were cut in a diameter of 14 mm, dried under vacuum at 120 °C for 12 h and introduced into an Ar-filled glovebox without air exposure.

Electrolyte Preparation: The choice of electrolyte followed this previous studies where graphite/K half cells showed the best capacity retention in an EC:DEC solvent mixture.[1,14] Mixtures containing propylene carbonate (PC) could not be used due to the incompatibility with graphite, although their anodic stability would be preferable. According to Hosaka and Komaba,[65] the EC:DEC-based electrolyte mixtures were the most widely used solvent in over 50% of all studies (based on 223 studies analyzed), which makes this electrolyte composition representative for a large number of studies. The electrolyte was 0.75 M KPF_6 dissolved in a mixture of EC:DEC (v/v = 1:1). The solution was stirred overnight in the glovebox to dissolve the electrolyte salt.

Cell assembly and testing: Cell cycling was performed either on a VMP-300 or a BCS battery cycler (both Biologic, France).

Graphite/K Half Cell Assembly: Coin cells with SUS304 steel-grade were used in this setup. For preparation of the potassium counter-reference electrode a piece of potassium was applied on a coin cell spacer and distributed homogenously with a ceramic knife and spatula. Each cell contained one Whatman and one Celgard separator, with the latter facing the graphite working electrode. The separators were soaked in 150 µL electrolyte and then sealed in a coin cell crimper.

The cells were cycled galvanostatically using a constant current (CC)-constant potential (CP) cycling protocol. For the first two cycles a rate of C/20 (1C = 279 mAh g^{-1} (KC_8)) was applied between the potential limits of 0.025 V and 1.20 V versus K^+/K. The cut-off condition during the CP-step was a limiting current of C/40 (half the current of the CC-step). On the following cycles the cycling rate was increased to C/10 and the limiting current in the CP-step was increased to an equivalent of C/20. One cell was only cycled for one cycle at C/20 and stopped after reaching the upper cut-off limit. The second cell continued to the tenth cycle, ending in the discharged state (deintercalated graphite).

Graphite/KFF Full Cell Assembly: It was paramount in this setup to use coin cells with SUS316L steel, for its higher corrosion resistance.[24] The graphite electrode, a Celgard/Whatman/Celgard separator stack and the KFF electrode were stacked on top of each other (N/P ratio ≈ 1.00–1.30), so that both electrodes faced a Celgard separator (to avoid contaminations from glassfibers). The separators were wetted with 150 µL electrolyte and then sealed in a coin cell crimper.

Galvanostatic cycling of graphite/KFF full cells was carried out similar to the half cell tests with a constant current (CC)-constant potential (CP) cycling protocol. On the initial two cycles a rate of C/20 (1C = 279 mAh g^{-1} (KC_8)) was applied between the voltage limits of 2.0 V and 4.15 V. The cut-off condition during the CP-step was a limiting current of C/40 (half the current of the CC-step). One cell was stopped after the first cycle after the lower cut-off limit was reached. For the cell that continued beyond the first cycle (to the 30th cycle) the cycling rate was increased to C/10 starting from the 3rd cycle. The limiting current in the CP-step was increased accordingly to an equivalent of C/20. The cell capacity was referred to the KFF active material mass (KFF reached a practical discharge capacity of $Q(KFF)_{discharge}$ = 120 mAh g^{-1} after the first cycle, as determined in this previous study[4]).

Data Processing: The galvanostatic cycling data was exported to TXT file extension using the EC-Lab software (V11.27) and further processed using the in-house developed «bat2dat» R package that was available on github.[66] Reported full cell capacities refer to the active material mass of the positive electrode.

Photoelectron spectroscopy (PES): PES was a highly surface-sensitive technique, probes the element-specific chemical environments of surface SEI species. Non-destructive PES depth profiling was carried out ex situ on cycled electrodes extracted from coin cells at three different photon energies (1487, 2150, 6450 eV) from in-house measurements and hard X-ray radiation at the BESSY II synchrotron facility in Berlin.

PES Depth Profiling Approach: In-depth probing of the SEI layer with PES requires variable excitation energies to vary the probing depth. The probing depth of in-house PES (i.e., X-ray photoelectron spectroscopy, XPS) with common excitation energies from Al-K_α (1486.6 eV) or Mg-K_α (1253.6 eV) X-ray sources was restricted to less than 10 nm,[34,35] which often was insufficient to probe through the entire SEI layer, the thickness of which can reach tens of nm.[67] The probing depth was a function of the inelastic mean free path (IMFP) of the generated photoelectrons and thus of their kinetic energy.[68] As a result, the probing depth increases with increasing the energy of photons used to excite photoelectrons from a specific orbital. Therefore, variation of the excitation energy was a means to perform non-destructive depth profiling of the electrode surface. The synchrotron radiation allows for varying and selecting the excitation energies over a wide range, e.g. at the KMC-1 beamline[69] at BESSY II between 2 keV to up to 10 keV, which was also equipped with High Kinetic Energy electron analyzer installed at the HIKE end station.[70] Compared to sputter depth profiling (e.g., Ar+ sputtering/etching) the surface layer remains intact, which removes the risk of generating sputter-induced degradation products.[35,70] Different etching rates of organic and generally more dense inorganic compounds can differ greatly (e.g., between potassium salts and many carbon species), thus generating rough surface topologies dominated by inorganic material. Unlike depth profiling with different photon energies, ion etching thus bears a high risk of altering the SEI stoichiometry.

Sample Preparation & Transfer: Cycled samples were collected after cell disassembly shortly after cycling stopped. In parallel, one cell of each configuration was put aside directly after assembly (without cycling) and stored at open circuit voltage (OCV) in the glovebox, so that the storage time matched the cycling time of the 10 and 30 cycles aged cells, respectively ("OCV samples"). The electrodes were then rinsed with DMC before they were cut into smaller pieces to fit the sample holders. In-house samples were mounted on the sample holder inside an Ar-filled glovebox and then transferred under inert gas conditions to the spectrometer. Measurements were conducted without charge neutralization. Synchrotron samples were fixed in plastic containers and then vacuum sealed (inside two

pouch bags) for transport. The sample bags were then opened in a Ar-filled glovebox located at BESSY, placed on the sample holders and mounted in the transfer chamber. The transfer chamber was then evacuated and attached to the load-lock of HIKE without air exposure.

General: The binding energy (BE) range of C1s spectra was extended to 310 eV, to include the K2p lines in the region between 290–300 eV. To assess possible beam-induced irradiation effects, F1s and P2p spectra were collected first. In addition, another F1s and C1s spectrum were recorded at the end of a measurement set.

In-House PES: X-ray photoelectron spectroscopy (XPS) measurements were performed on a Thermo Scientific K-alpha spectrometer using monochromatized Al Kα radiation (1486.6 eV, 400 µm spot size). Photoemission spectra were recorded with a concentric hemispherical analyzer at a pass energy of 50 eV.

Hard X-ray Photoelectron Spectroscopy (HAXPES): Graphite and KFF electrodes were examined by hard X-ray radiation (2150 eV & 6450 eV (3rd order) excitation energy) at the high kinetic energy electron (HIKE) spectrometer endstation located at BESSY II's KMC-1 beamline at HZB.[70] Spectra were collected with a Scienta R4000 analyzer and a pass energy of 200 eV. At the higher photon energy, measurement of the K1s and P1s core levels was conducted rather than the K2s and P2p core levels, due to the poor photoionization cross-section of the latter at this excitation energy.[67]

Data Analysis: Spectra of graphite electrodes were referenced to the C 1s peak (C-C/C-H) at 285.0 eV binding energy. For KFF electrode the F1s line at 688.1 eV of PVdF (-CH_2-CF_2-) was used for referencing. Analysis of in-house data was performed with Avantage (software version 5.9904, Thermo Scientific). The fitted data was then exported to IGOR Pro (v6.37, WaveMaterics Inc.) for data curation and plotting. Synchrotron data was directly imported to IGOR Pro. The dimension of the spectra was reduced from 2D to 1D by collapsing the data along the kinetic energy axis. A Shirley background function was used during data processing. The spectra were fitted with Voigt profiles (Lorentzian contribution of 20%). The asymmetry in the graphite peak shape was fitted with an decaying exponential tail.[71] Quantification was performed for spectra recorded at 1487 eV and 2150 eV. For the in-house spectra (1487 eV), the instrument specific sensitivity factors were obtained during fitting in Avantage. Relative sensitivity factors for the synchrotron data were determined following the method detailed in ref. [65] and were reported in Table S1 (Supporting Information): The normalized peak areas for each spectral component, $A(i)_{norm}$ were then obtained from the respective fitted peak area A(i) and the product of IMPF,[72,73] core level cross-sections (CS) from ref[33,74] (under consideration of the measurement geometry) and the transmission function (TF) of HIKE at the respective kinetic energies equation 1,

$$A(i)_{norm} = \frac{A(i)}{CS \cdot IMPF \cdot TF} \quad (1)$$

The quantification in Avantage (in-house data), also used an kinetic energy dependent correction factor (energy compensation factor, EC provided in Avantage) for the depth-dependent inelastic scattering of photoelectrons in a homogenous layer (adjusted escape depth), as follows

$$A(i)_{norm} = \frac{A(i)}{CS \cdot TF \cdot EC} \quad (2)$$

The atomic concentration, [i] (at.%), was calculated as (equation 3),

$$[i] = \frac{A(i)_{norm}}{\sum A(i)_{norm}} \cdot 100\% \quad (3)$$

Supporting Information

Supporting Information is available from the Wiley Online Library or from the author.

Acknowledgements

This work contributes to the research performed at CELEST (Center for Electrochemical Energy Storage Ulm-Karlsruhe) and was funded by the German Research Foundation (DFG) under Project ID 390874152 (POLiS Cluster of Excellence, EXC 2154) and #448719339. The authors thank HZB for the allocation of synchrotron radiation beamtime (Proposal Nr. 212–10605). The Energy Materials In Situ Laboratory Berlin (EMIL) was acknowledged for providing the infrastructure to allow for sample preparation in Ar glovebox and air-free transfer to HIKE.

Open access funding enabled and organized by Projekt DEAL.

Conflict of Interest

The authors declare no conflict of interest.

Data Availability Statement

The data that support the findings of this study are openly available in Zenodo at https://doi.org/10.5281/zenodo.12803066, reference number.[62]

Keywords

Graphite, HAXPES, KIB, photoelectron spectroscopy, potassium, prussian white, XPS

Received: August 23, 2024
Revised: September 10, 2024
Published online: September 20, 2024

[1] F. Jeschull, J. Maibach, *Electrochem. Commun.* **2020**, *121*, 106874.
[2] S. Komaba, T. Hasegawa, M. Dahbi, K. Kubota, *Electrochem. Commun.* **2015**, *60*, 172.
[3] P. A. Morozova, I. A. Trussov, D. P. Rupasov, V. A. Nikitina, A. M. Abakumov, S. S. Fedotov, *Crystals* **2021**, *11*, 895.
[4] A. D. Khudyshkina, P. A. Morozova, A. J. Butzelaar, M. Hoffmann, M. Wilhelm, P. Theato, S. S. Fedotov, F. Jeschull, *ACS Appl. Polym. Mater.* **2022**, *4*, 2734.
[5] C. Xu, F. Jeschull, W. R. Brant, D. Brandell, K. Edström, T. Gustafsson, *J. Electrochem. Soc.* **2018**, *165*, A40.
[6] W. R. Brant, R. Mogensen, S. Colbin, D. O. Ojwang, S. Schmid, L. Häggström, T. Ericsson, A. Jaworski, A. J. Pell, R. Younesi, *Chem. Mater.* **2019**, *31*, 7203.
[7] K. Hurlbutt, S. Wheeler, I. Capone, M. Pasta, *Joule* **2018**, *2*, 1950.
[8] A. J. Naylor, M. Carboni, M. Valvo, R. Younesi, *ACS Appl. Mater. Interfaces* **2019**, *11*, 45636.
[9] T. Hosaka, T. Matsuyama, R. Tatara, Z. T. Gossage, S. Komaba, *Chem. Sci.* **2023**, *14*, 8860.
[10] T. Hosaka, S. Komaba, *Bull. Chem. Soc. Jpn.* **2022**, *95*, 569.
[11] F. Allgayer, J. Maibach, F. Jeschull, *ACS Appl. Energy Mater.* **2022**, *5*, 1136.
[12] L. Madec, V. Gabaudan, G. Gachot, L. Stievano, L. Monconduit, H. Martinez, *ACS Appl. Mater. Interfaces* **2018**, *10*, 34116.
[13] L. Caracciolo, L. Madec, H. Martinez, *ACS Appl. Energy Mater.* **2021**, *4*, 11693.
[14] A. Hofmann, F. Müller, S. Schöner, F. Jeschull, *Battery Supercaps* **2023**, *6*, 202300325.
[15] L. Caracciolo, L. Madec, G. Gachot, H. Martinez, *ACS Appl. Mater. Interfaces* **2021**, *13*, 57505.
[16] T. Hosaka, T. Fukabori, T. Matsuyama, R. Tatara, K. Kubota, S. Komaba, *ACS Energy Lett.* **2021**, *6*, 3643.

[17] I. Panasenko, M. Bäuerle, F. Jeschull, *SSRN* **2024**.
[18] K. Ciosek Högström, S. Malmgren, M. Hahlin, M. Gorgoi, L. Nyholm, H. Rensmo, K. Edström, *Electrochim. Acta* **2014**, *138*, 430.
[19] K. Ciosek Högström, M. Hahlin, S. Malmgren, M. Gorgoi, H. Rensmo, K. Edström, *J. Phys. Chem. C* **2014**, *118*, 12649.
[20] F. Jeschull, J. Maibach, R. Félix, M. Wohlfahrt-Mehrens, K. Edström, M. Memm, D. Brandell, *ACS Appl. Energy Mater.* **2018**, *1*, 5176.
[21] H. Wang, H. Wang, S. Chen, B. Zhang, G. Yang, P. Gao, J. Liu, X. Fan, Y. Huang, J. Lin, Z. Shen, *ACS Appl. Energy Mater.* **2019**, *2*, 7942.
[22] B. Larhrib, L. Madec, L. Monconduit, H. Martinez, *J. Power Sources* **2023**, *588*, 233743.
[23] Z. T. Gossage, T. Hosaka, T. Matsuyama, R. Tatara, S. Komaba, *J. Mater. Chem. A* **2023**, *11*, 914.
[24] A. Smith, P. Stüble, L. Leuthner, A. Hofmann, F. Jeschull, L. Mereacre, *Battery Supercaps* **2023**, *6*, 202300080.
[25] B. Larhrib, L. Madec, *Battery Supercaps* **2023**, *6*, 202300061.
[26] A. Hofmann, F. Müller, S. Schöner, F. Jeschull, *Battery Supercaps* **2023**, *6*, 20230032.
[27] B. Larhrib, L. Madec, L. Monconduit, H. Martinez, *Electrochim. Acta* **2022**, *425*, 140747.
[28] B. Larhrib, L. Madec, *Batter. Supercaps* **2023**, *6*, 1.
[29] F. Jeschull, L. Zhang, Ł. Kondracki, F. Scott, S. Trabesinger, *J. Phys. Energy* **2023**, *5*, 025003.
[30] K. U. Schwenke, S. Solchenbach, J. Demeaux, B. L. Lucht, H. A. Gasteiger, *J. Electrochem. Soc.* **2019**, *166*, A2035.
[31] J. Stadler, C. Krupp, M. Ecker, J. Bandlow, B. Spier, A. Latz, *J. Power Sources* **2022**, *521*, 230952.
[32] J. Zhu, M. S. Dewi Darma, M. Knapp, D. R. Sørensen, M. Heere, Q. Fang, X. Wang, H. Dai, L. Mereacre, A. Senyshyn, X. Wei, H. Ehrenberg, *J. Power Sources* **2020**, *448*, 227575.
[33] M. B. Trzhaskovskaya, V. K. Nikulin, V. I. Nefedov, V. G. Yarzhemsky, *At. Data Nucl. Data Tables* **2006**, *92*, 245.
[34] L. R. Painter, E. T. Arakawa, M. W. Williams, J. C. Ashley, *Radiat. Res.* **1980**, *83*, 1.
[35] H. Shinotsuka, S. Tanuma, C. J. Powell, D. R. Penn, *Surf. Interface Anal.* **2019**, *51*, 427.
[36] S. Malmgren, K. Ciosek, M. Hahlin, T. Gustafsson, M. Gorgoi, H. Rensmo, K. Edström, *Electrochim. Acta* **2013**, *97*, 23.
[37] F. Jeschull, H. Q. Pham, A. Ghamlouche, P. K. Thakur, S. Trabesinger, J. Maibach, *J. Phys. Energy* **2023**, *5*, 025002.
[38] B. S. Parimalam, A. D. MacIntosh, R. Kadam, B. L. Lucht, *J. Phys. Chem. C* **2017**, *121*, 22733.
[39] F. Lindgren, C. Xu, J. Maibach, A. M. Andersson, M. Marcinek, L. Niedzicki, T. Gustafsson, F. Björefors, K. Edström, *J. Power Sources* **2016**, *301*, 105.
[40] A. V. Naumkin, A. Kraut-Vass, S. W. Gaarenstroom, C. J. Powell, "NIST X-ray Photoelectron Spectroscopy Database," **2012**.
[41] J. C. Green, P. Decleva, *Coord. Chem. Rev.* **2005**, *249*, 209.
[42] A. V. Plakhotnyk, L. Ernst, R. Schmutzler, *J. Fluor. Chem.* **2005**, *126*, 27.
[43] R. Mogensen, J. Maibach, W. R. Brant, D. Brandell, R. Younesi, *Electrochim. Acta* **2017**, *245*, 696.
[44] G. G. Eshetu, T. Diemant, M. Hekmatfar, S. Grugeon, R. J. Behm, S. Laruelle, M. Armand, S. Passerini, *Nano Energy* **2019**, *55*, 327.
[45] F. Jeschull, J. Maibach, K. Edström, D. Brandell, *J. Electrochem. Soc.* **2017**, *164*, A1765.
[46] G. G. Eshetu, S. Grugeon, H. Kim, S. Jeong, L. Wu, G. Gachot, S. Laruelle, M. Armand, S. Passerini, *ChemSusChem* **2016**, *9*, 462.
[47] T. Sasaki, T. Abe, Y. Iriyama, M. Inaba, Z. Ogumi, *J. Power Sources* **2005**, *150*, 208.
[48] H. Kim, S. Grugeon, G. Gachot, M. Armand, L. Sannier, S. Laruelle, *Electrochim. Acta* **2014**, *136*, 157.
[49] G. Gachot, S. Grugeon, M. Armand, S. Pilard, P. Guenot, J. M. Tarascon, S. Laruelle, *J. Power Sources* **2008**, *178*, 409.
[50] C. L. Campion, W. Li, B. L. Lucht, *J. Electrochem. Soc.* **2005**, *152*, A2327.
[51] J. Henschel, J. L. Schwarz, F. Glorius, M. Winter, S. Nowak, *Anal. Chem.* **2019**, *91*, 3980.
[52] J. Zhao, B. Jagger, L. F. Olbrich, J. Ihli, S. Dhir, M. Zyskin, X. Ma, M. Pasta, *ACS Energy Lett.* **2024**, *9*, 1537.
[53] S. Dhir, B. Jagger, A. Maguire, M. Pasta, *Nat. Commun.* **2023**, *14*, 3833.
[54] D. Schäfer, K. Hankins, M. Allion, U. Krewer, F. Karcher, L. Derr, R. Schuster, J. Maibach, S. Mück, D. Kramer, R. Mönig, F. Jeschull, S. Daboss, T. Philipp, G. Neusser, J. Romer, K. Palanisamy, C. Kranz, F. Buchner, R. J. Behm, A. Ahmadian, C. Kübel, I. Mohammad, A. Samoson, R. Witter, B. Smarsly, M. Rohnke, *Adv. Energy Mater.* **2024**, *14*, 2302830.
[55] F. Jeschull, *ChemElectroChem* **2024**,*11*, 202400254.
[56] X. Yi, H. Fu, A. M. Rao, Y. Zhang, J. Zhou, C. Wang, B. Lu, *Nat. Sustain.* **2024**, *7*, 326.
[57] Y. Geng, H. Fu, Y. Hu, A. M. Rao, L. Fan, J. Zhou, B. Lu, *Appl. Phys. Lett.* **2024**, *124*, 063901.
[58] H. Onuma, K. Kubota, S. Muratsubaki, T. Hosaka, R. Tatara, T. Yamamoto, K. Matsumoto, T. Nohira, R. Hagiwara, H. Oji, S. Yasuno, S. Komaba, *ACS Energy Lett.* **2020**, *5*, 2849.
[59] J. Maibach, F. Jeschull, D. Brandell, K. Edström, M. Valvo, *ACS Appl. Mater. Interfaces* **2017**, *9*, 12373.
[60] L. Gehrlein, C. Leibing, K. Pfeifer, F. Jeschull, A. Balducci, J. Maibach, *Electrochim. Acta* **2022**, *424*, 140642.
[61] D. Stottmeister, L. Wildersinn, J. Maibach, A. Hofmann, F. Jeschull, A. Groß, *ChemSusChem* **2023**, *17*, 202300995.
[62] L. A. Ma, A. J. Naylor, L. Nyholm, R. Younesi, *Angew. Chem.* **2021**, *133*, 4905.
[63] A. D. Khudyshkina, A. J. Butzelaar, Y. Guo, M. Hoffmann, T. Bergfeldt, M. Schaller, S. Indris, M. Wilhelm, P. Théato, F. Jeschull, *Electrochim. Acta* **2023**, *454*, 142421.
[64] A. D. Khudyshkina, U.-C. Rauska, A. J. Butzelaar, M. Hoffmann, M. Wilhelm, P. Theato, F. Jeschull, *Battery Supercaps* **2024**, *7*, 202300404.
[65] N. Mallik, J. Hajhemati, M. Frégnaux, D. Coutancier, T. Ashish, Z. Shan-ting, C. Hartmann, E. Hüsam, A. Saleh, T. Vincent, O. Fournier, R. G. Wilks, D. Aureau, R. Félix, N. Schneider, M. Bär, P. Schulz, *Nano Energy* **2024**, *126*, 109582.
[66] F. Jeschull, **2022**, https://github.com/fabje223/bat2dat.
[67] B. Philippe, M. Hahlin, K. Edström, T. Gustafsson, H. Siegbahn, H. Rensmo, *J. Electrochem. Soc.* **2016**, *163*, A178.
[68] A. Klein, T. Mayer, A. Thissen, W. Jaegermann, in *Methods Phys. Chem*, Wiley-VCH Verlag GmbH & Co. KGaA, Weinheim, Germany **2012**, p. 477.
[69] F. Schaefers, M. Mertin, M. Gorgoi, *Rev. Sci. Instrum.* **2007**, *78*, 123102.
[70] M. Gorgoi, S. Svensson, F. Schäfers, G. Öhrwall, M. Mertin, P. Bressler, O. Karis, H. Siegbahn, A. Sandell, H. Rensmo, W. Doherty, C. Jung, W. Braun, W. Eberhardt, *Nucl. Instruments Methods Phys. Res. Sect. A Accel. Spectrometers, Detect. Assoc. Equip.* **2009**, *601*, 48.
[71] G. H. Major, T. G. Avval, D. I. Patel, D. Shah, T. Roychowdhury, A. J. Barlow, P. J. Pigram, M. Greiner, V. Fernandez, A. Herrera-Gomez, M. R. Linford, *Surf. Interface Anal.* **2021**, *53*, 689.
[72] S. Tanuma, C. J. Powell, D. R. Penn, *Surf. Interface Anal.* **1994**, *21*, 165.
[73] S. Tougaard, **2016**.
[74] M. B. Trzhaskovskaya, V. I. Nefedov, V. G. Yarzhemsky, *At. Data Nucl. Data Tables* **2001**, *77*, 97.
[75] F. Jeschull, E. Kataev, I. Panasenko, C. Njel, R. Félix, J. Maibach, *Zenodo* **2024**, https://doi.org/10.5281/zenodo.12803066.